

Physically Consistent Variational Denoising of Image Fluid Flow Estimates ^{*}

Andrey Vlasenko, Christoph Schnörr

Image and Pattern Analysis Group, Heidelberg Collaboratory for Image Proc.(HCI),
University of Heidelberg, Germany, {vlasenko,schnoerr}@math.uni-heidelberg.de

Abstract. High-speed image measurements of fluid flows define an important field of research in experimental fluid mechanics and the related industry. Numerous competing methods have been developed for both 2D and 3D measurements. Estimates of fluid flow velocity fields are often corrupted, however, due to various deficiencies of the imaging process, making the physical interpretation of the measurements questionable. We present an algorithm that accepts vector field estimates from any method and returns a physically plausible denoised version of it. Our approach enforces the physical structure and does not rely on particular noise models. Accordingly, the algorithm performs well for different types of noise and estimation errors. The computational steps are sufficiently simple to scale up to large 3D problems in the near future.

1 Introduction

Experimental fluid mechanics is a challenging field of research of imaging science with important industrial applications [1]. During the last two decades, the prevailing technique for investigating turbulent flows through imaging has been particle image velocimetry in 2D [2, 3], whereas various 3D measurement techniques, while being attractive from the physical viewpoint of applications, have been suffering from various drawbacks including noisy measurements, complexity and costs of the set-up, and limited resolution [4–9]. Remarkable progress has been recently achieved through a novel technique, Tomographic Particle Image Velocimetry (TomoPIV) [10] that, in principle, provides 3D estimates with higher spatial resolution.

As a result, there are a range of methods for computing vector field estimates of incompressible viscous flows from image data, that exhibit diverse artefacts depending on the particular technique used, and on the particular physical scenario considered. This motivates to investigate a method that denoises a given vector field in a *physically plausible* way. Rather than to model noise explicitly which is difficult and too specific due to the diversity of estimation errors that can occur, the method should return a vector field that is close to the input data and approximately satisfies the basic physical equations governing the flow. At

^{*} This work has been supported by the German Science Foundation, priority program 1147, grant SCHN 457/6-3.

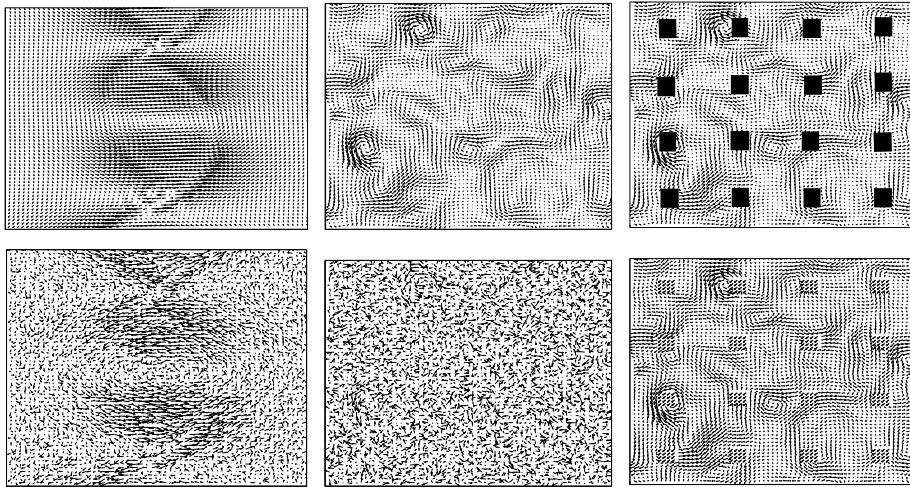


Fig. 1. Top: Two ground truth flows, a Kelvin-Helmholtz flow (**left**) and a turbulent flow (**top center**). **Bottom left, center:** The Kelvin-Helmholtz and turbulent flows spoiled with noise. **Right column:** The turbulent flow corrupted by missing data and outliers within rectangular regions. The location of these regions is assumed to be *unknown*. The problem addressed in this paper is to restore the flows in a way that takes into account the physical origin of the flows but does not depend on a particular noise model. In the case of missing data (lower right panel), we assume these regions to be *unknown*.

the same time, the method should be robust to various types of estimation errors and computationally simple, so as to be applicable to large-scale 3D problems that the next generation of 3D measurement techniques will raise in the near future.

Our approach presented below is motivated by recent work on *variational PIV methods*. Ruhnau and Schnörr [11] showed how to estimate *physically consistent* flow from PIV image sequences utilizing a distributed-parameter control approach. This has been extended in [12, 13] to a dynamic setting based on the vorticity transport equation formulation of the Navier-Stokes equation.

The task studied in this paper is more involved, however, because we wish to process corrupted vector fields as input data, and therefore cannot resort to image data in order to determine additional control variables. Rather, we wish to devise a method that accepts vector field estimates produced by *any* of the algorithms mentioned above, and returns a denoised version just by preserving and enforcing physically consistent flow structure.

Our paper is organized as follows. We introduce the basic notation and the overall variational approach in section 2. Additional details for each computational stage involved are provided in section 3. Experimental results for various error types and performance measures are discussed on section 4. We conclude and point out further work in section 5.

2 Variational Approach

2.1 Notation, Preliminaries

We formulate our approach for the 3D case. Vectors are indicated with bold font. \mathbf{v} denotes a velocity field and $\boldsymbol{\omega} = \nabla \times \mathbf{v}$ its vorticity. The 2D case is automatically obtained by setting $\mathbf{v} = (v_1, v_2, 0)^\top$. For example, $\nabla \times \mathbf{v}$ then yields a vorticity field $\boldsymbol{\omega} = (0, 0, \omega_3)^\top$, with scalar vorticity $\omega_3 = \partial_{x_1} v_2 - \partial_{x_2} v_1$.

We denote by $\langle \mathbf{u}, \mathbf{v} \rangle, \|\mathbf{v}\|$ the euclidean inner product and norm, and by $\langle \mathbf{u}, \mathbf{v} \rangle_\Omega, \|\mathbf{v}\|_\Omega$ the inner product and norm of $[L^2(\Omega)]^d$, $d = 2, 3$, respectively, where $\Omega \subset \mathbb{R}^d$ is the given image section.

We list few relations used in the remainder of this paper. The vorticity-transport equation reads

$$\frac{\partial}{\partial t} \boldsymbol{\omega} + (\mathbf{v} \cdot \nabla) \boldsymbol{\omega} + (\boldsymbol{\omega} \cdot \nabla) \mathbf{v} = \nu \Delta \boldsymbol{\omega} . \quad (1)$$

We consider a flow on a such short time interval, that the scale of temporal vorticity changes becomes several orderer smaller, than the scale of spatial vorticity changes. The term $\partial_t \boldsymbol{\omega}$ in (1) has a negligible impact in comparison with impacts of other terms, and it can be omitted from the equation. In other words, the the chosen time interval is short enough, that one can reduce the flow motion to a quasi stationary case. Once the time derivative was excluded, we can focus on a fixed point of time. For the remaining left-hand side, we introduce the short-hand

$$\mathbf{e}(\mathbf{v}) = \nu \Delta \boldsymbol{\omega} , \quad \mathbf{e}(\mathbf{v}) = (\mathbf{v} \cdot \nabla) \boldsymbol{\omega} + (\boldsymbol{\omega} \cdot \nabla) \mathbf{v} . \quad (2)$$

The integral identity

$$\int_{\Omega} (\nabla \times \mathbf{v}) \cdot \boldsymbol{\phi} \, dx - \int_{\Omega} \mathbf{v} \cdot (\nabla \times \boldsymbol{\phi}) \, dx = 0 , \quad \forall \boldsymbol{\phi} \in [C_0^\infty(\Omega)]^d , \quad (3)$$

is used to derive Euler-Lagrange equations below, and for incompressible flow we have

$$\nabla \times \nabla \times \boldsymbol{\omega} = -\Delta \boldsymbol{\omega} . \quad (4)$$

2.2 Approach

Suppose we have given a corrupted vector field \mathbf{d} . The true underlying viscous flow is incompressible and is assumed to satisfy (2). Regarding the design of a denoising algorithm, we have to keep in mind computational simplicity in order to be able to solve sequences of large-scale 3D problems that sensors will produce in the near future.

Iterative Algorithm. In view of these requirements, we study in this paper a denoising approach comprising the following steps:

1. Project the data \mathbf{d} to the subspace of divergence-free flows: $\mathbf{d} \rightarrow \mathbf{v}$.
2. Compute the vorticity $\boldsymbol{\omega}_{\mathbf{v}} = \nabla \times \mathbf{v}$. Preserve and enforce physically plausible flow structure in terms of equation (2): $\boldsymbol{\omega}_{\mathbf{v}} \rightarrow \boldsymbol{\omega}$.
3. Recover velocity from vorticity: $\boldsymbol{\omega} \rightarrow \mathbf{u}$.

If the termination criterion is satisfied, stop. Otherwise, continue with step 1. The steps 1.-3. will be detailed in section 3.

Termination criterion. We compute the energy spectrum¹ in term of the Fourier transform $\widehat{\|\mathbf{v}\|^2}(\mathbf{k})$, $\mathbf{k} \in [\pi, \pi]^d$, and define the magnitude of a cutoff frequency k_c depending on the flow under investigation, e.g. in terms of the smallest scale of vorticities to be resolved. We stop the iteration once the upper energy band has been sufficiently damped relative to the lower band

$$\int_{\|\mathbf{k}\|_{\infty} \geq k_c} \widehat{\|\mathbf{v}\|^2}(\mathbf{k}) d\mathbf{k} \leq c_k \int_{\|\mathbf{k}\|_{\infty} \leq k_c} \widehat{\|\mathbf{v}\|^2}(\mathbf{k}) d\mathbf{k}, \quad (5)$$

where a typical value is $c_k = 100$. See Fig. 2 below for an illustration.

3 Computational Steps: Details

3.1 Subspace Projection

Consider the orthogonal decomposition of the space $\mathbf{V} = [L^2(\Omega)]^3 = \mathbf{V}_g \oplus \mathbf{V}_{sol}$ into gradients and solenoidal (divergence-free) vector fields [14]: $\mathbf{d} = \nabla\phi + \nabla \times \boldsymbol{\psi}$. The orthogonal projection $P : \mathbf{V} \rightarrow \mathbf{V}_{sol}$ onto the space

$$\mathbf{V}_{sol} = \{\mathbf{v} \in V \mid \nabla \cdot \mathbf{v} = 0, \mathbf{v} \cdot \mathbf{n} = 0 \text{ on } \partial\Omega\}$$

is accomplished by solving $\Delta\phi = \nabla \cdot \mathbf{d}$, $\phi = 0$ on $\partial\Omega$ and removing the divergence

$$\mathbf{v} = \mathbf{d} - \nabla\phi \in \mathbf{V}_{sol}. \quad (6)$$

3.2 Vorticity Rectification

Set $\boldsymbol{\omega}_{\mathbf{v}} = \nabla \times \mathbf{v}$. In order to take into account Eqn. (2), we minimize

$$\min_{\boldsymbol{\omega}} \left\{ \|\boldsymbol{\omega} - \boldsymbol{\omega}_{\mathbf{v}}\|_{\Omega}^2 + \alpha \left(\nu \|\nabla \times \boldsymbol{\omega}\|_{\Omega}^2 + 2 \langle \mathbf{e}(\mathbf{v}), \boldsymbol{\omega} \rangle_{\Omega} \right) \right\} \quad (7)$$

The first term ensures that the minimizer stays close to the vorticity computed in the previous step, and the second term enforces (2). Computing the first

¹ Note that the usual definition is based on time averages. We focus in this paper on a single time point, however.

variation of the functional (7) and applying (3) and (4), we obtain the Euler-Lagrange equation

$$\boldsymbol{\omega} - \alpha\nu\Delta\boldsymbol{\omega} = \boldsymbol{\omega}_{\mathbf{v}} - \alpha\mathbf{e}(\mathbf{v}) .$$

This is a system of linear diffusion equations (a single equation in 2D). Rewriting this equation,

$$\boldsymbol{\omega} = \boldsymbol{\omega}_{\mathbf{v}} - \alpha(\mathbf{e}(\mathbf{v}) - \nu\Delta\boldsymbol{\omega}) ,$$

we see that the vorticity $\boldsymbol{\omega}$ is corrected by the residual of Eqn. (2) where the nonlinearity $\mathbf{e}(\mathbf{v})$ is evaluated at \mathbf{v} computed in the preceding step. Because correct boundary conditions are not known, we reduce the Laplacian at $\partial\Omega$ to linear diffusion *along* the boundary.

3.3 Velocity Restoration

The minimizer $\boldsymbol{\omega}$ of the previous step may not correspond to a solenoidal vector field. Hence, as a third computational step, we propose to minimize

$$\min_{\mathbf{u}} \left\{ \|\mathbf{u} - \mathbf{v}\|_{\Omega}^2 + \beta\|\nabla \times \mathbf{u} - \boldsymbol{\omega}\|_{\Omega}^2 \right\} , \quad (8)$$

with \mathbf{v} from (6) and $\boldsymbol{\omega}$ from (7). Computing the first variation of the functional (8) and applying (4), we obtain again a linear diffusion system

$$\mathbf{u} - \beta\Delta\mathbf{u} = \mathbf{v} + \beta\nabla \times \boldsymbol{\omega} , \quad \frac{\partial\mathbf{u}}{\partial\mathbf{n}} = 0 .$$

Here, it is plausible to impose natural boundary conditions on \mathbf{u} .

4 Experiments and Discussion

We tested the denoising approach for 2D flows, so far. The 3D case is subject of future work and will be reported elsewhere. The test was carried out for two different flows:

- A Kelvin-Helmholtz flow [15], [16], see Fig. 1 top-left and Fig. 3 top, that occurs when velocity shear is present withing a continuous fluid, or when there is a sufficiently large velocity difference across the interface between two fluids.
- A turbulent flow from Navier-Stokes simulations, see Fig. 1 top-right and Fig. 4 top.

Various types of data corruptions were investigated: White Gaussian noise with both high and low signal-to-noise ratio as well as square regions with missing and corrupted data. Figure 1 displays these vector fields represented by \mathbf{d} in the first step (6) of our iterative restoration approach.

Denote \mathbf{g} :ground truth flow, \mathbf{d} : corrupted input data, \mathbf{u} : denoised vector field. In order to evaluate the denoising performance of our approach and its robustness we used the following quantitative performance measures:

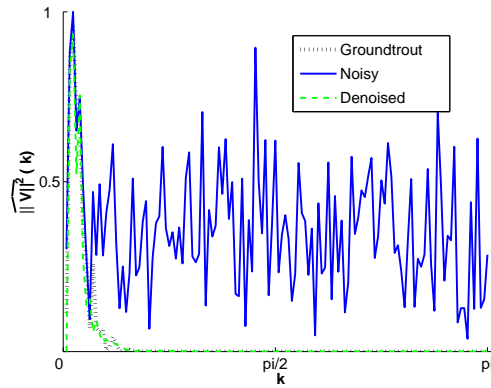


Fig. 2. Illustration of the termination criterion (5) for the noisy turbulent flow experiment shown in Fig. 4. Restoration effectively removes noise and preserves physically significant large-scale structures of vorticity.

$$SDR = \frac{\|\mathbf{d}-\mathbf{g}\|_{\Omega}}{\|\mathbf{u}-\mathbf{g}\|_{\Omega}}, \quad ADR = \frac{\|\arccos(\widehat{\mathbf{d}\mathbf{g}})\|_{\Omega}}{\|\arccos(\widehat{\mathbf{u}\mathbf{g}})\|_{\Omega}}, \quad NDR = \frac{\|\mathbf{d}\|_{\Omega}}{\|\mathbf{g}\|_{\Omega}}, \quad DDR = \frac{\|\mathbf{u}\|_{\Omega}}{\|\mathbf{g}\|_{\Omega}}.$$

The meanings of these measures are as follows: SDR gives the rate between standard deviations of noisy and denoised vector fields from groundtruth vector field, FDR gives the rate between average angle deviations of noisy and denoised data from groundtruth, ADR gives the rate of average angle deviation of noisy and denoised vector fields from groundtruth, NDR and DDR give the average vector length of noisy and denoised vector fields in comparison with groundtruth average vector length.

Figures 3-5 confirm and illustrate that the algorithm does not depend on a particular model of noise and errors. Rather, the physical structures (vorticity) are restored fairly well. Quantitative results are given in the figure captions.

Figure 4 shows an example of very low signal-to-noise-ratio. The still plausible restoration result illustrates that our approach gracefully degrades with increasing noise levels, and its limitation: Small-scale structures cannot always be correctly restored in such extreme situations.

5 Conclusion

We presented a black-box variational approach to the restoration of PIV-measurements in experimental fluid mechanics. It restores physically significant flow structures, copes with various types of noise and errors, degrades gracefully with decreasing signal-to-noise ratio and involves computationally simple steps.

Our further work will further explore the trade-off between computational simplicity (i.e. efficiency) and tighter couplings of the computational steps through constraints, and on problem representations specific to large-scale 3D applications.

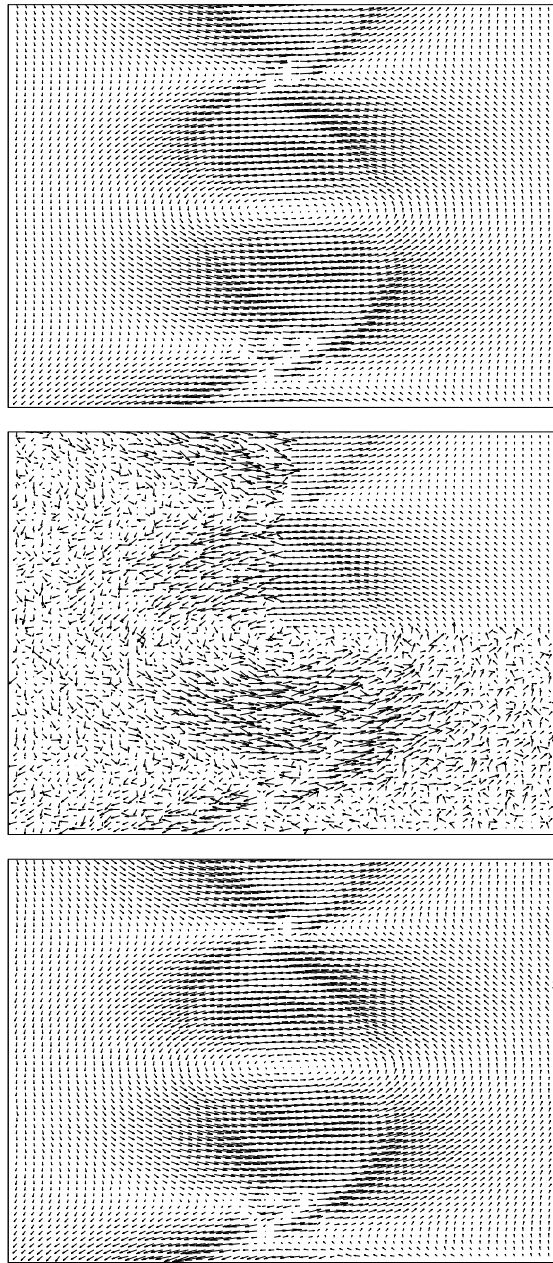


Fig. 3. Top: Ground truth flow \mathbf{g} . **Center:** Noisy data \mathbf{d} . Noise has been cut out within a rectangular region to illustrate the signal-to-noise ratio. **Bottom:** Denoised flow \mathbf{u} . Performance measure: SDR=4.43, ADR=6032, NDR=1.12, DDR=0.999. Number of iterations: 3

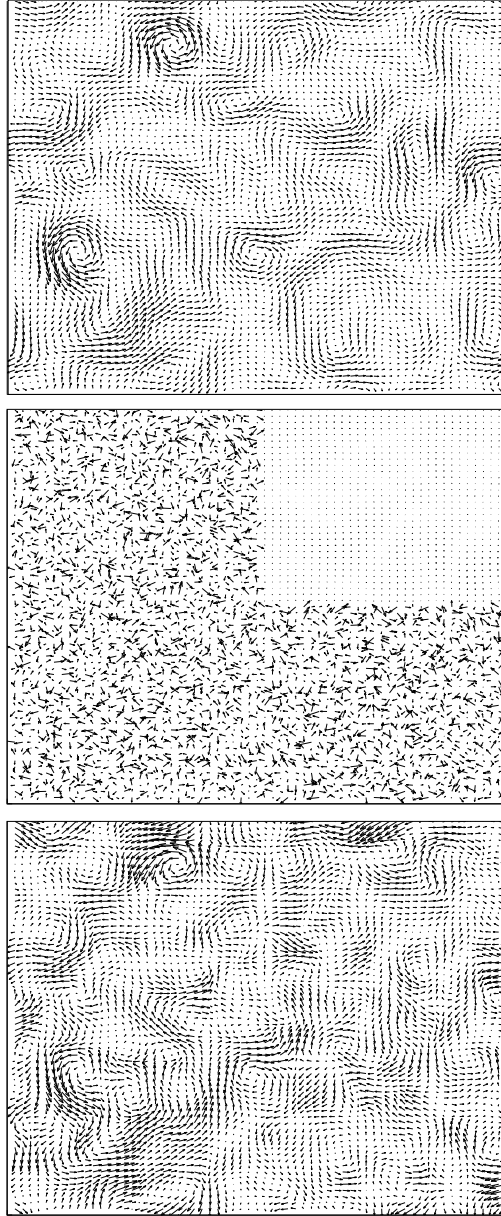


Fig. 4. Top: Ground truth flow \mathbf{g} . **Center:** Noisy data. Noise has been cut out within a rectangular region to illustrate the signal-to-noise ratio. **Bottom: d.** Denoised flow \mathbf{u} . Performance measures: SDR=15.12, ADR=2.45, NDR=9.51, DDR=1.004. Number of iterations: 16. This example shows that the approach gracefully degrades with increasing noise levels and its limitation: In the extreme situation above, not all small-scale structures can be restored.

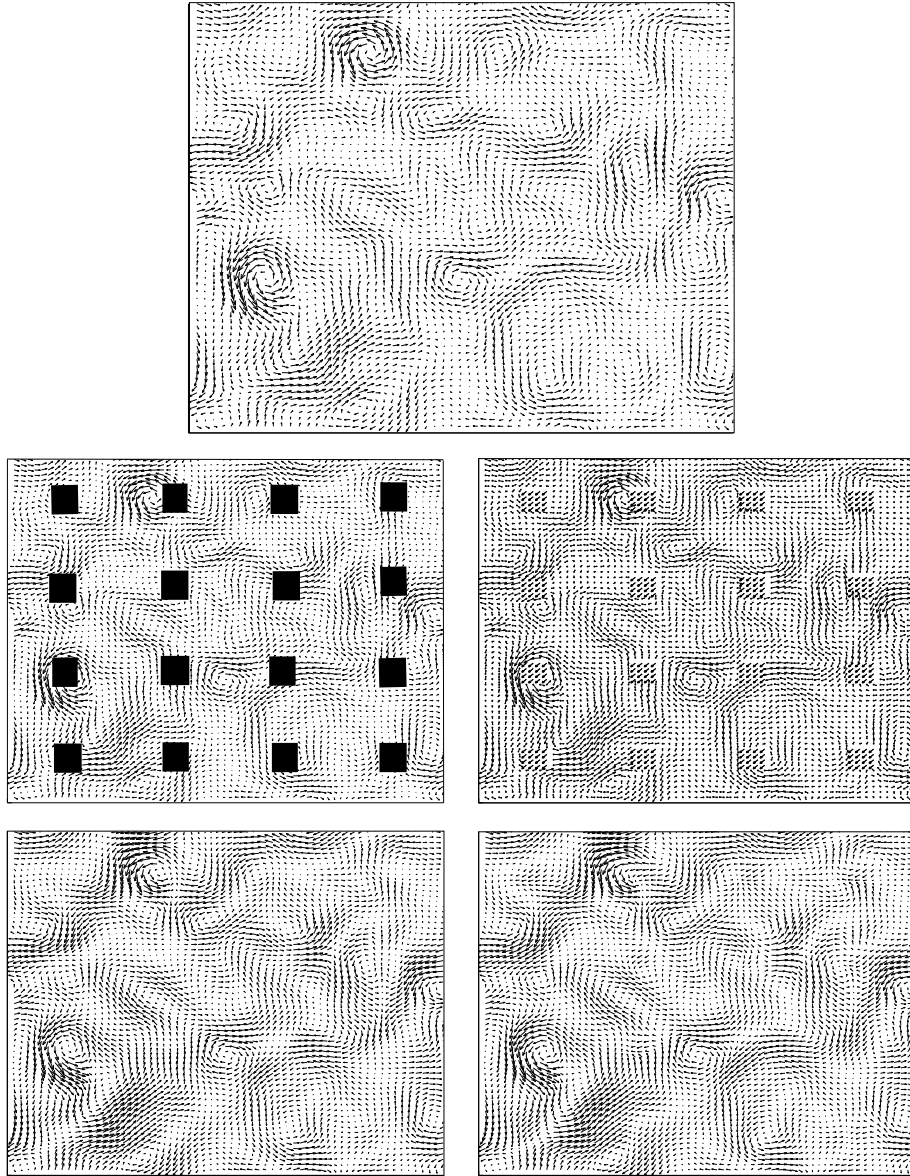


Fig. 5. Top: Ground truth flow \mathbf{g} . **Center:** Corrupted data \mathbf{d} by missing values (**left**) or outliers within rectangular regions (**right**). The location of these regions are assumed to be *unknown*. **Bottom:** Denoised flows \mathbf{u} . Performance measures, left experiment: SDR=1.1131, DDR=1.128. Number of iterations: 4. Performance measures, right experiment: SDR=1.645, ADR=0.532, NDR=1.0087, DDR=0.924. Number of iterations $k=5$.

References

1. C. Tropea, A.L. Yarin, and J.F. Foss, editors. *Springer Handbook of Experimental Fluid Mechanics*. Springer, 2007.
2. R.J. Adrian. Twenty years of particle velocimetry. *Experiments in Fluids*, 39(2):159–169, 2005.
3. M. Raffel, C.E. Willert, S.T. Wereley, and J. Kompenhans. *Particle Image Velocimetry – A Practical Guide*. Springer, 2007.
4. C. Brücker. Digital-particle-image-velocimetry (DPIV) in a scanning light-sheet: 3d starting flow around a short cylinder. *Experiments in Fluids*, 19(4), 1995.
5. S. Burgmann, C. Brücker, and W. Schröder. Scanning PIV measurements of a laminar separation bubble. *Experiments in Fluids*, 41(2):319–326, 2006.
6. K.D. Hinsch. Holographic particle image velocimetry. *Measurement Science and Technology*, 13:61–72, 2002.
7. H.G. Maas, A. Gruen, and D. Papantoniou. Particle tracking velocimetry in three-dimensional flows. *Experiments in Fluids*, 15(2):133–146, 1993.
8. K. Hoyer, M. Holzner, B. Lüthi, M. Guala, A. Liberzon, and W. Kinzelbach. 3d scanning particle tracking velocimetry. *Experiments in Fluids*, 39(5):923–934, 2005.
9. P. Ruhnau, C. Güttler, T. Putze, and C. Schnörr. A variational approach for particle tracking velocimetry. *Measurement Science and Technology*, 16:1449–1458, 2005.
10. G. Elsinga, F. Scarano, B. Wieneke, and B. van Oudheusden. Tomographic particle image velocimetry. *Experiments in Fluids*, 41(6):933–947, 2006.
11. P. Ruhnau and C. Schnörr. Optical stokes flow estimation: An imaging-based control approach. *Exp. Fluids*, 42:61–78, 2007. in press.
12. P. Ruhnau, A. Stahl, and C. Schnörr. On-line variational estimation of dynamical fluid flows with physics-based spatio-temporal regularization. In *Pattern Recognition – 28th DAGM Symposium*, volume 4174 of *LNCS*, pages 444–454. Springer, 2006.
13. P. Ruhnau, A. Stahl, and C. Schnörr. Variational estimation of experimental fluid flows with physics-based spatio-temporal regularization. *Measurement Science and Technology*, 18:755–763, 2007.
14. V. Girault and P.-A. Raviart. *Finite Element Methods for Navier-Stokes Equations*. Springer, 1986.
15. N. Stashchuk, V. Vlasenko, and K. Hutter. Kelvin-Helmholz instability: Numerical modelling of disintegration of basin-scale internal waves in a tank filled with stratified water. *Nonlinear Processes in Geophysics*, 12:955–964, 2005.
16. M. Van Dyke. *An Albumn of Fluid Motion*. The Parabolic Press, Stanford, CA, 1982.